TECHNICAL REPORTS

nature neuroscience

A genetically targeted optical sensor to monitor calcium signals in astrocyte processes

Eiji Shigetomi[1], Sebastian Kracun[1], Michael V Sofroniew[2] & Baljit S Khakh[1,2]

Calcium signaling is studied as a potential form of astrocyte excitability that may control astrocyte involvement in synaptic and cerebrovascular regulation. Fundamental questions remain unanswered about astrocyte calcium signaling, as current methods can not resolve calcium in small volume compartments, such as near the cell membrane and in distal cell processes. We modified the genetically encoded calcium sensor GCaMP2 with a membrane-tethering domain, Lck, increasing the level of Lck-GCaMP2 near the plasma membrane tenfold as compared with conventional GCaMP2. Using Lck-GCaMP2 in rat hippocampal astrocyte-neuron cocultures, we measured near-membrane calcium signals that were evoked pharmacologically or by single action potential–mediated neurotransmitter release. Moreover, we identified highly localized and frequent spontaneous calcium signals in astrocyte somata and processes that conventional GCaMP2 failed to detect. Lck-GCaMP2 acts as a genetically targeted calcium sensor for monitoring calcium signals in previously inaccessible parts of astrocytes, including fine processes.

© 2010 Nature America, Inc. All rights reserved.

Astrocytes tile the CNS, exert essential support functions[1], provide energy metabolites to neurons[2], and respond to injury and disease[3]. In addition, evidence suggests that astrocytes participate in synaptic function[4] and regulate blood flow to meet demands set by neuronal activity[5,6]. The combination of timescale and cellular architecture involved in these responses suggests that certain astrocyte functions are regulated by rapid signaling events in distal processes that contact synapses or blood vessels.

Astrocytes display excitability in the form of intracellular calcium concentration increases that have been recorded *in vitro*[7], *in vivo*[8–13] and in brain slices from humans[14]. Astrocyte calcium transients occur spontaneously and are increased by neuronal activity[15]. As calcium is a ubiquitous second messenger, astrocyte calcium elevations may control communication with other cells. Communication between astrocytes and neurons is particularly intriguing because individual astrocytes contact many thousands of synapses[16,17] and because electrophysiological and imaging studies demonstrate the synaptic consequences of second messenger signaling in astrocyte processes[18].

Physiological experiments suggest two settings in which astrocytes and neurons may communicate. First, calcium levels in astrocytes are elevated in response to neurotransmitters released from neurons[19]. Second, increases in astrocyte calcium cause the release of glutamate, which in turn affects neurons[20,21]. These data suggest that calcium-dependent 'gliotransmitter' release leads to short- and long-term changes in neuronal and synaptic function[18,22]. Nevertheless, calcium-dependent astrocyte-to-neuron signaling is still debated and there is evidence both for[20,21,23,24] and against it[25,26] being a prevalent feature of CNS circuits. These issues have been discussed extensively[15,27–30], raising awareness of the need for improved methods to selectively activate, silence and monitor astrocyte calcium signals.

Recent work has suggested that somatic calcium signals may be an unreliable measure of astrocyte excitability and its downstream signaling[31]. The controversy on the role of astrocyte calcium signals in influencing neuronal function may also be rooted in the fact that most experimental evidence stems from calcium measurements in somatic compartments, which is paradoxical when one considers that astrocytes are thought to signal at a local level via their distal processes[18,29]. This situation exists because current methods can not measure calcium in small volume compartments such as astrocyte processes, which are too meager to adequately load with organic calcium indicator dyes[29], although pioneering attempts have found distributed glial calcium signaling[32,33].

A direct method for monitoring calcium signals in astrocyte processes is needed to elucidate if, when, where and how astrocytes affect neurons. Buoyed by recent advances using genetic targeting to achieve selective astrocyte ablation[34], silencing of exocytosis[35], as well as blockade[26] and activation[25] of astrocyte calcium signals, we developed a genetic strategy for monitoring real-time astrocyte calcium signaling selectively in near-membrane regions and processes.

RESULTS

Global and near-membrane calcium signals

Protoplasmic astrocytes are known to have fine branches *in vivo* and it is thought that they signal locally in processes[29]. One problem in the study of astrocyte calcium signaling has been the inability to measure calcium in astrocyte processes with organic calcium indicator dyes[29]. Moreover, it is commonly assumed that a change in astrocyte calcium measured globally reflects similar changes near the plasma membrane, although this has not been directly investigated.

Using rat hippocampal astrocyte-neuron cocultures, we studied spontaneous astrocyte calcium transients with epifluorescence (EPI) and total internal reflection fluorescence (TIRF) microscopy[36],

[1]Department of Physiology, David Geffen School of Medicine, University of California Los Angeles, Los Angeles, USA. [2]Department of Neurobiology, David Geffen School of Medicine, University of California Los Angeles, Los Angeles, USA. Correspondence should be addressed to B.S.K. (bkhakh@mednet.ucla.edu).

Received 29 October 2009; accepted 15 April 2010; published online 23 May 2010; doi:10.1038/nn.2557

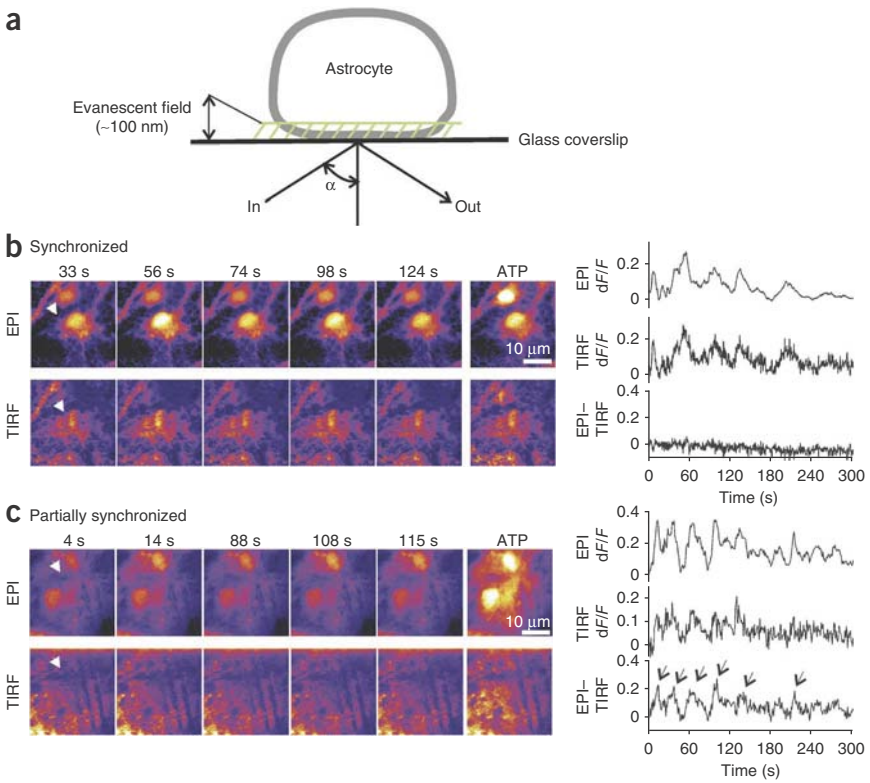

Figure 1 Simultaneous imaging of global and near-membrane calcium in astrocytes. (**a**) Diagram illustrates the principal of TIRF, whereby an evanescent field illuminates a restricted area of the cell. Fluo-4 was excited by an argon laser for TIRF (488 nm) or a monochromator for EPI microscopy (488 nm). (**b**) Representative images of an astrocyte loaded with Fluo-4 under EPI and TIRF microcopy, where the calcium transients were synchronous between these imaging modalities. The arrowhead indicates an ROI, which corresponds to the traces (d*F*/*F* over time) on the right. All calcium transients observed were synchronized between EPI and TIRF, resulting in a flat trace when the normalized TIRF traces were subtracted from the normalized EPI traces. (**c**) Data are presented as in **b** for an astrocyte that showed nonsynchronized events between EPI and TIRF microscopy. In this case, subtraction resulted in a peaky trace. Arrows indicate calcium signals that were observed in EPI. In both **b** and **c**, ATP caused a uniform increase in calcium.

which measure global and near-membrane calcium signals, respectively[36] (**Fig. 1a**). We observed that 48% of 211 calcium transients (from 33 astrocytes) measured globally also elevated calcium near the plasma membrane in 10 ms; we referred to these as synchronized events. This was readily visible by subtracting the normalized EPI and TIRF traces, resulting in a flat trace (**Fig. 1b**). However, 50% of 211 calcium transients measured globally failed to elevate calcium near the plasma membrane; we referred to these as EPI unique events and the cells in which they occurred as being partially synchronized (**Fig. 1c**). A further 2% of 211 events only elevated calcium near the plasma membrane (these were not examined further). In contrast with the differences observed for spontaneous calcium signals, application of 30 μM ATP to activate astrocyte $P2Y_1$ receptors increased calcium globally and near the membrane (**Fig. 1b**,**c**). On average, the EPI unique events were smaller and briefer than the synchronous ones (d*F*/*F* values of 5 ± 4 and 30 ± 6% and half duration values of 5.4 ± 0.9 and 8.4 ± 1.0 s for EPI unique and synchronous events, respectively). Using ratiometric Fura-2 imaging[37], we estimated the change in cytosolic calcium concentration in three different conditions (**Fig. 2a**,**b**), spontaneous calcium signals (n = 50) and for signals evoked by 1 and 30 μM ATP (n = 65 and 103, respectively). We then repeated these experiments using Fluo-4 and measured d*F*/*F* values for spontaneous and 1 and 30 μM ATP-evoked calcium signals (n = 207, 18 and 56, respectively). Using both datasets, we determined a proportionality constant between the Fluo-4 and Fura-2 signals and used this to estimate the change in calcium concentration. Thus, synchronous events elevated calcium in the cytosol by ~300–400 nM, whereas EPI unique events elevated calcium in the cytosol by less than ~100 nM.

We examined the ability of G protein–coupled receptor (GPCR) agonists to elevate calcium globally and near the membrane of astrocytes. We used ATP (30 μM), glutamate (300 μM), DHPG (10 μM), TFLLR (30 μM) and ET-1 (100 nM), which are agonists of $P2Y_1$, mGluR, group I mGluR, PAR-1 and endothelin-1 receptors, respectively. We also used FLRFa (5 μM) as an agonist of heterologously expressed MrgA1 receptors[25]. In each case, the GPCR agonists elevated calcium levels globally and near the membrane with similar kinetics. Taken together, these experiments suggest that global measures of spontaneous astrocyte calcium transients do not accurately reflect calcium dynamics near the membrane and GPCR agonists do not mimic spontaneous astrocyte calcium signals in terms of amplitude (**Fig. 2c**) or spread to the plasma membrane (**Fig. 2**). We sought to develop an approach for measuring calcium in small volumes of astrocytes such as near the membrane and in fine processes.

GCaMP2 fails to measure spontaneous calcium signals

GCaMP2 is a genetically encoded green fluorescent protein (GFP)-based calcium indicator that increases its fluorescence yield when calcium ions bind to the M13 and CaM fragments[38,39] (**Fig. 3a**). We used GCaMP2 because it is excited and emits at a single wavelength (488 and 508 nm, respectively) and has a calcium affinity of ~150 nM, close to that of organic calcium indicator dyes that have been used in past studies of astrocyte calcium signaling[29]. In addition, GCaMP2 kinetics are suited to astrocytes, which have transients that exist on a timescale of seconds[15] (**Figs. 1** and **2**).

We expressed GCaMP2 in astrocytes to determine whether we could measure spontaneous calcium transients. GCaMP2 was robustly expressed in astrocytes (**Supplementary Video 1**), but we failed to detect any spontaneous calcium transients in eight of eight cells with EPI or TIRF microscopy (imaged for 5 min each; **Supplementary Video 1**). We could, however, measure calcium elevations triggered by bath applications of GPCR agonists in all cells (for example, 30 μM ATP; **Supplementary Video 2**). From these data, we concluded that cytosolic GCaMP2 was not suitable for monitoring spontaneous astrocyte calcium transients.

Membrane targeted Lck-GCaMP2

One way to improve GCaMP2 is to optimize it through mutagenesis, but another approach is to target GCaMP2 to the plasma membrane, effectively increasing its local expression in a restricted volume. This should improve the signal-to-noise ratio, as the reporter would be in the plane of the membrane in which calcium fluxes may be maximal. Cognizant of previous experiences with membrane tethers[40],

© 2010 Nature America, Inc. All rights reserved.

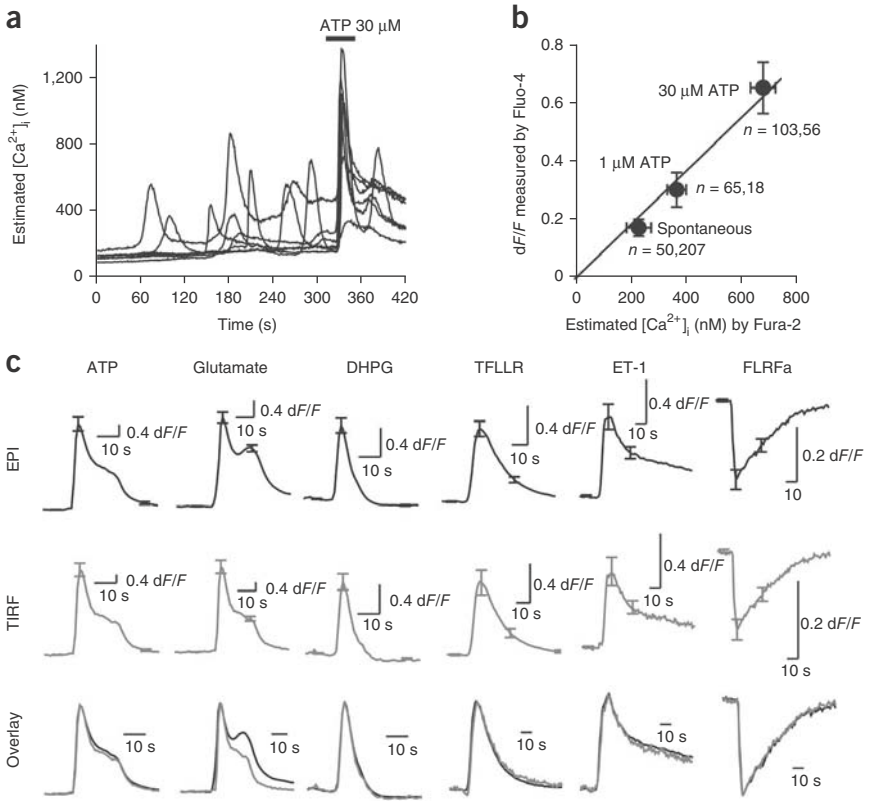

Figure 2 Quantification of spontaneous and pharmacologically evoked calcium signals measured by TIRF and EPI microscopy. (**a**) Representative traces of calcium transients observed using Fura-2; 30 μM ATP was applied for the duration indicated by the bar (~30 s). (**b**) Relationship between d*F*/*F* measured with Fluo-4 and estimated calcium measured with Fura-2. (**c**) Agonist-induced calcium transients observed in EPI and TIRF (top, averaged EPI traces; middle, averaged TIRF traces; bottom, normalized traces). We used 30 μM ATP ($n = 54$), 300 μM glutamate ($n = 54$), 10 μM DHPG (group I mGluR agonist, $n = 65$), 30 μM TFLLR (PAR1 agonist, $n = 59$), 100 nM endothelin-1 (ET-1, $n = 45$) and 5 μM FLRF amide (MrgA1 receptor agonist, $n = 13$). As a result of spectral overlap, we used Fura-Red for calcium imaging of MrgA1-EGFP–transfected astrocytes (2 d after transfection); thus, the traces are downward for these experiments. Error bars represent s.e.m.

we used the N-terminal domain of Lck, a Src tyrosine kinase, which is known to contain tandem palmitoylation and myristoylation domains[41,42].

We engineered GCaMP2 to carry the N-terminal 26 residue tag that we refer to as the Lck domain to generate Lck-GCaMP2 (**Fig. 3a**), burying an N-terminal arginine residue that could render GCaMP2 susceptible to degradation[43]. For initial expression analysis and characterization, we expressed Lck-GCaMP2 in HEK-293 cells (**Fig. 3**). In contrast with the cytosolic fluorescence of GCaMP2 (**Fig. 3b**), we observed fluorescence that was localized to the edges of cells with Lck-GCaMP2 (**Fig. 3c**). Lck-GCaMP2 also provided fluorescence measurements of calcium ion concentration with a Ca^{2+} K_d of 168 ± 27 nM and Hill slope of 4.0 ± 1.0 ($n = 9$; **Fig. 3d**), close to reported values for GCaMP2 (ref. 39).

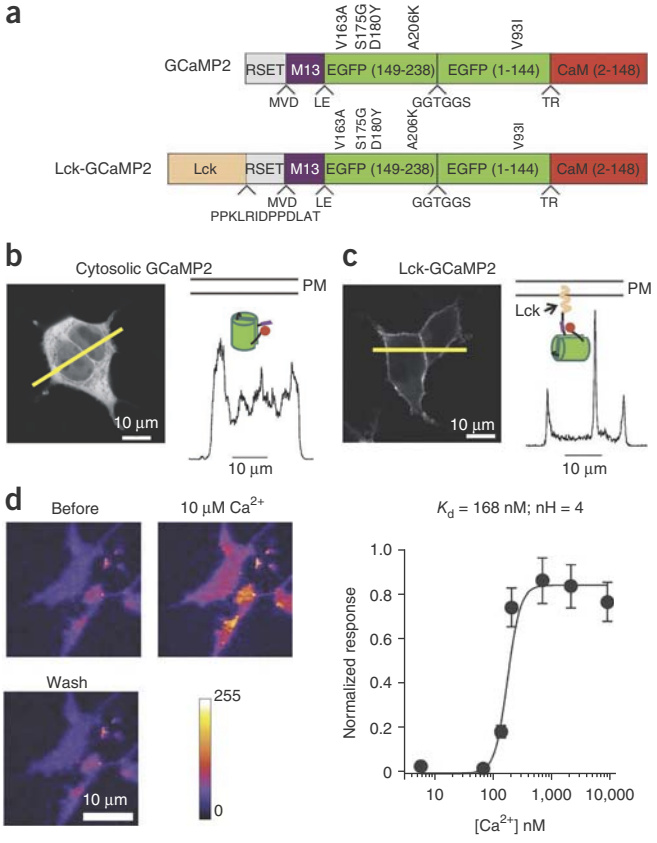

Lck-GCaMP2 measures global astrocyte calcium signals

We expressed Lck-GCaMP2 in astrocytes and determined whether it was uniformly expressed in the membrane (**Supplementary Fig. 1**) by comparing TIRF images of astrocytes expressing Lck-GCaMP2 to those of cells expressing Lck-GFP and to astrocytes labeled with the membrane dye FM1-43. In all three cases, the TIRF images were similar, with no obvious puncta (**Supplementary Fig. 1**), indicating that Lck-GCaMP2 was uniformly distributed in the membrane.

We determined whether Lck-GCaMP2 could measure GPCR activation in astrocytes using ATP as a $P2Y_1$ agonist (**Figs. 1**, **2** and **4a**) by employing rapid switching[44] between TIRF and EPI to compare the signals measured globally and near the membrane of astrocytes expressing Lck-GCaMP2. We found that the ATP–evoked calcium signals measured with EPI and

Figure 3 Design and characterization of Lck-GCAMP2. (**a**) Schematic representation of cytosolic GCaMP2 and membrane targeted Lck-GCaMP2. The membrane-tethering Lck domain was added to N terminus of GCaMP2. (**b**) Representative image and line profile of two HEK-293 cells expressing cytosolic GCaMP2; the inset cartoon shows cytosolic GCaMP2 in relation to the plasma membrane (PM, representative of $n = 5$ fields of view). The colors in the cartoon correspond to the colors in **a**. (**c**) Data are presented as in **b** for Lck-GCaMP2; note that the fluorescence was strongly located at the edges of the cells, near the membrane (representative of $n = 5$ fields of view). (**d**) HEK cells permeablized with 0.1% Triton X-100 for 15–30 s, before, during and after application of buffered solutions containing 10 μM free calcium ions. Right, calcium sensitivity of Lck-GCaMP2 measured in this way ($n = 9$). Error bars represent s.e.m.

© 2010 Nature America, Inc. All rights reserved.

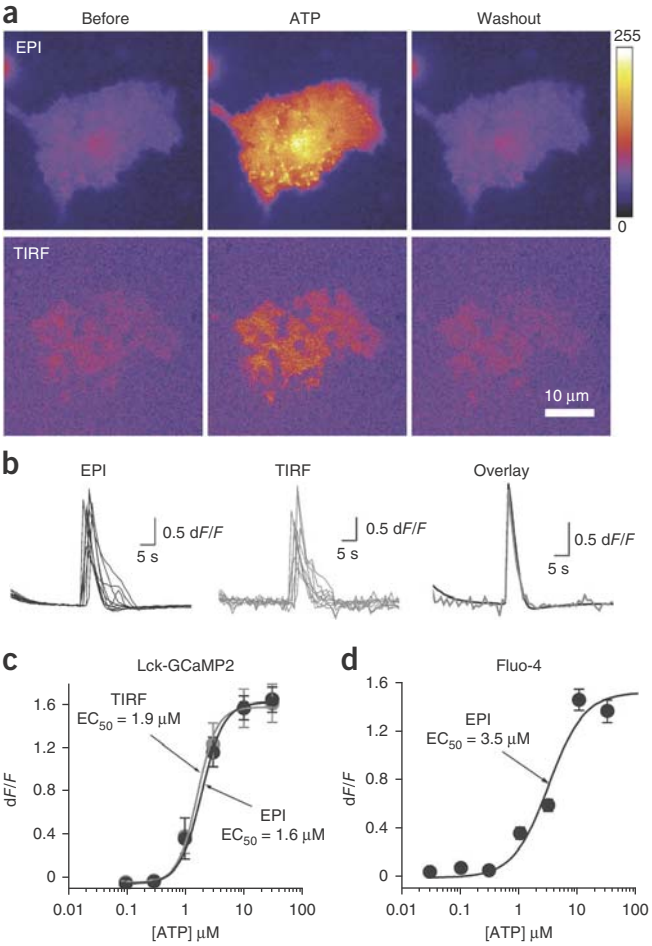

Figure 4 ATP-evoked calcium signals in astrocytes measured with Lck-GCaMP2. (**a**) Upper panels show a Lck-GCaMP2–expressing astrocyte imaged with EPI microscopy. The lower panels show the footprint of the same cell imaged 10 ms later with TIRF. The EPI images are brighter than the TIRF images because this mode of illumination reports on the entire cell and because the EPI excitation was brighter. When these factors are corrected for, the expression of Lck-GCaMP2 is extremely robust in the plasma membrane (by TIRF; **Supplementary Fig. 7**). Representative images are shown before, during and after applications of 30 μM ATP. (**b**) Representative traces for ATP-evoked changes in fluorescence measured in astrocytes with EPI and TIRF microscopy. Right, superimposed traces measured with EPI and TIRF from the same astrocyte. (**c**) Dose-response curves for ATP measured with EPI ($n = 10$) and TIRF ($n = 10$) microscopy from astrocytes expressing Lck-GCaMP2. (**d**) ATP dose-response curve for astrocytes loaded with Fluo-4 ($n = 28$–54). Error bars represent s.e.m.

TIRF microscopy were almost identical in their time course (**Fig. 4b**) and that the signals had the same ATP sensitivity, with half-maximal effective concentration (EC_{50}) values of ~2 μM (EPI, 1.6 ± 0.2 μM; TIRF, 1.9 ± 0.2 μM; $n = 10$) and Hill slopes of ~2.6 (EPI, 2.6 ± 0.3; TIRF, 2.3 ± 0.1; $n = 10$; **Fig. 4b**,**c**). These values are similar to the ATP EC_{50} of 3.5 μM ($n = 28$–54) measured with Fluo-4 (**Fig. 4d**).

Lck-GCaMP2 measures neuron-to-astrocyte signaling

We used hippocampal astrocyte-neuron cocultures to determine whether Lck-GCaMP2 could measure signaling mediated by neurotransmitter release from neurons onto astrocytes[29]. We applied 1–180 action potentials at 30 Hz using electrical field stimulation (EFS) and plotted the change in fluorescence measured from astrocytes expressing Lck-GCaMP2 using EPI microscopy (**Fig. 5a**,**b**). The peak d*F*/*F* was related to the number of action potentials between 1 and 60. In 7 of 11 astrocytes, a single action potential caused substantial increases in Lck-GCaMP2 fluorescence (0.37 ± 0.09, $n = 7$), which lasted 19.2 ± 4.8 s (quantified as $T_{0.5}$). The EFS-evoked signals were reproducible when EFS was applied every 5 min (**Fig. 5**).

We repeated the EFS experiments with tetrodotoxin (TTX, 1 μM, $n = 5$) or Cd^{2+} (100 μM, $n = 5$) in the bath solution to block voltage-dependent sodium and calcium channels, respectively, and found that the EFS-evoked fluorescence changes were abolished (**Fig. 5c**–**e**). On the basis of previous findings[45], we examined whether ATP was released during EFS from neurons to mediate calcium signals in

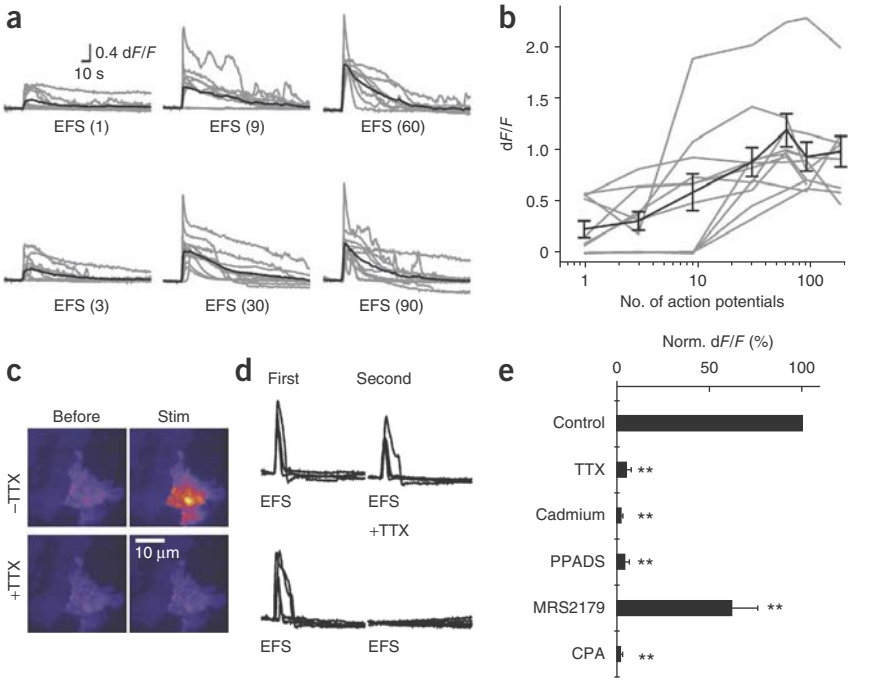

Figure 5 Responses of astrocytes expressing Lck-GCaMP2 during EFS of neurons. (**a**) Traces from 11 astrocytes (gray), their averages superimposed (black), showing the Lck-GCaMP2 response during EFS. The number of action potentials applied is indicated in brackets. (**b**) The graphs plot the relationship between the change in fluorescence of Lck-GCaMP2 and the number of action potentials for individual cells (gray) and their average (black). (**c**) Representative images of an astrocyte expressing Lck-GCaMP2 gathered with EPI microscopy, before and during EFS under control conditions (top) and in the presence of 1 μM TTX (bottom). (**d**) Representative traces for five cells when EFS was applied twice (top) and when the second period of EFS was applied in the presence of 1 μM TTX. (**e**) Average data for experiments such as those shown in **c** and **d**. In these experiments, the second period of EFS was preceded by 10-min incubation with 1 μM TTX, 100 μM Cd^{2+}, 30 μM PPADS, 20 μM MRS2179 and 20 μM CPA. EFS consisted of 90 action potentials triggered in 3 s at 30 Hz. Error bars represent s.e.m. $^{**}P < 0.01$.

© 2010 Nature America, Inc. All rights reserved.

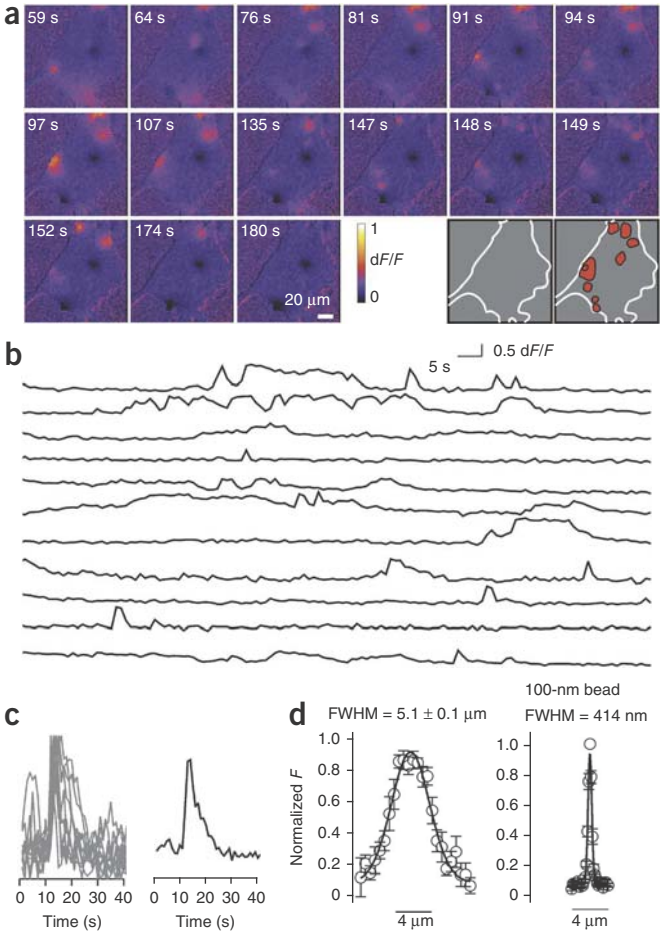

Figure 6 Spontaneous calcium signals measured with Lck-GCaMP2. (**a**) Time series of an astrocyte expressing Lck-GCaMP2. Numerous spotty calcium signals were observed. The gray cartoons show the outline of the astrocyte with the location of the spots superimposed. (**b**) Intensity versus time profile of 11 ROIs from images such as those shown in **a**. Note, calcium signals can be measured repeatedly in the same ROI. (**c**) Time course of ten spotty signals and the average in black. (**d**) The FWHM of the events ($n = 6$) and 100-nm beads ($n = 10$). Error bars represent s.e.m.

astrocytes. PPADS, a broad spectrum P2Y receptor antagonist, completely abolished the EFS-evoked signals (30 µM, $n = 5$; **Fig. 5e**). This is consistent with previous results on the functional expression of $P2Y_1$ receptors in astrocytes[29]. Consistent with this, the $P2Y_1$ receptor antagonist MRS2179 substantially decreased the responses evoked by EFS by ~40% (20 µM, $n = 10$; **Fig. 5e**). Moreover, the EFS-evoked responses were abolished when intracellular calcium stores were depleted with cyclopiazonic acid (CPA, 20 µM, $n = 4$).

Lck-GCaMP2 measures localized calcium signals

In contrast with cytosolic GCaMP2 (**Supplementary Video 1**), we readily monitored spontaneous astrocyte calcium transients using Lck-GCaMP2 and EPI microscopy. We observed numerous brief and spotty calcium signals in astrocytes, events that we referred to as microdomains (**Fig. 6a**,**b** and **Supplementary Videos 3** and **4**). By marking the area covered by each microdomain over 2 min of recording (**Fig. 6a**), we determined that they covered 23 ± 8% ($n = 8$) of the astrocyte surface. Microdomains occurred randomly, independently of each other, repeatedly at the same location and displayed kinetics on a timescale of seconds (**Fig. 6c**). The somatic microdomains had a full-width half maxima (FWHM) of 5.1 ± 0.1 µm ($n = 6$), greater than the point spread function of our microscope (~0.4 µm; **Fig. 6d**).

Many microdomains (~80%) were in astrocyte cell bodies, with the remainder being present in astrocyte processes that extended >20 µm (**Fig. 7a**). These latter microdomains were spatially and temporally distinct from somatic events (**Fig. 7a**), but we found no substantial differences between microdomains in somata and processes in terms of dF/F, $T_{0.5}$ and frequency (**Supplementary Table 1**). On average, we recorded 4.1 ± 1.6 microdomain locations per astrocyte ($n = 8$), with a mean $T_{0.5}$ of 3.9 ± 0.3 s ($n = 408$), a peak dF/F of 0.50 ± 0.01 ($n = 515$) and a frequency of 0.8 ± 0.07 events min^{-1} (159 microdomains, 56 cells).

Astrocytes in culture are flat, whereas they are more branched *in situ*. To recapitulate this more elaborate morphology, we treated the cells with 5 mM db-cAMP for 48 h, as this is known to cause astrocytes to extend processes[46] (**Supplementary Fig. 2** and **Supplementary Video 5**). We readily detected spontaneous Lck-GCaMP2 fluorescence increases in these extended processes that were very similar to those in cells that were not treated with db-cAMP (**Fig. 7b** and **Supplementary Table 1**). The spontaneous signals occurred up to 86 µm from the astrocyte cell body with a mean distance of 39 ± 5 µm ($n = 22$; **Fig. 7b**). This is consistent with the length of astrocyte processes found *in situ*, between 17–51 µm[47], indicating that Lck-GCaMP2 can report localized calcium signals in processes that are similar in length to those in intact preparations (**Fig. 7b** and **Supplementary Table 1**).

In contrast with the EFS-evoked signals (**Fig. 5**), microdomains were insensitive to 1 µM TTX ($n = 6$; **Fig. 8a**). We also found that CPA (20 µM, $n = 12$) completely abolished ATP-evoked calcium transients (**Fig. 8**) but spared the microdomains ($n = 21$) measured with Lck-GCaMP2 (**Fig. 8b**,**d**). Conversely, we found that microdomains were abolished in calcium-free extracellular buffers ($n = 20$), whereas the ATP-evoked responses persisted ($n = 10$; **Fig. 8c**,**d**). Moreover, incubation with the ATP receptor antagonist PPADS abolished ATP-evoked signals ($n = 11$) but had no effect on microdomains (10 µM, $n = 16$; **Fig. 8d**). Finally, activation of $P2Y_1$ and PAR1 GPCRs, alone or together, robustly elevated global calcium levels[31], but failed to affect the frequency of microdomain calcium signals (**Supplementary Fig. 3**). Taken together, these experiments provide strong evidence that microdomain calcium signals are independent of GPCR activation and calcium release from intracellular stores but are dependent on transmembrane calcium fluxes. Our data clearly show that Lck-GCaMP2 can be used to non-invasively monitor global (**Fig. 4**), pharmacologically evoked (**Fig. 4**), electrically evoked (**Fig. 5**) and spontaneous calcium signals in astrocytes (**Figs. 6–8**).

Further controls and characterization of Lck-GCaMP2

We imaged Lck-GCaMP2–expressing hippocampal neurons to determine whether astrocyte microdomain calcium signals were cell specific (**Supplementary Fig. 4** and **Supplementary Table 1**) and found several similarities and differences between neurons and astrocytes. First, ATP failed to evoke calcium signals in neurons but did so in astrocytes. In contrast, glutamate evoked similar signals in neurons and astrocytes (**Supplementary Fig. 4** and **Supplementary Table 1**). Second, we did not detect any spontaneous microdomains in nine of ten neurons (**Supplementary Fig. 4**, **Supplementary Video 6** and **Supplementary Table 1**), whereas we were readily able to observe microdomains in astrocytes (**Supplementary Table 1**). Third, where spontaneous calcium signals were detected (one of ten neurons), they were abolished by 1 µM TTX. In contrast,

© 2010 Nature America, Inc. All rights reserved.

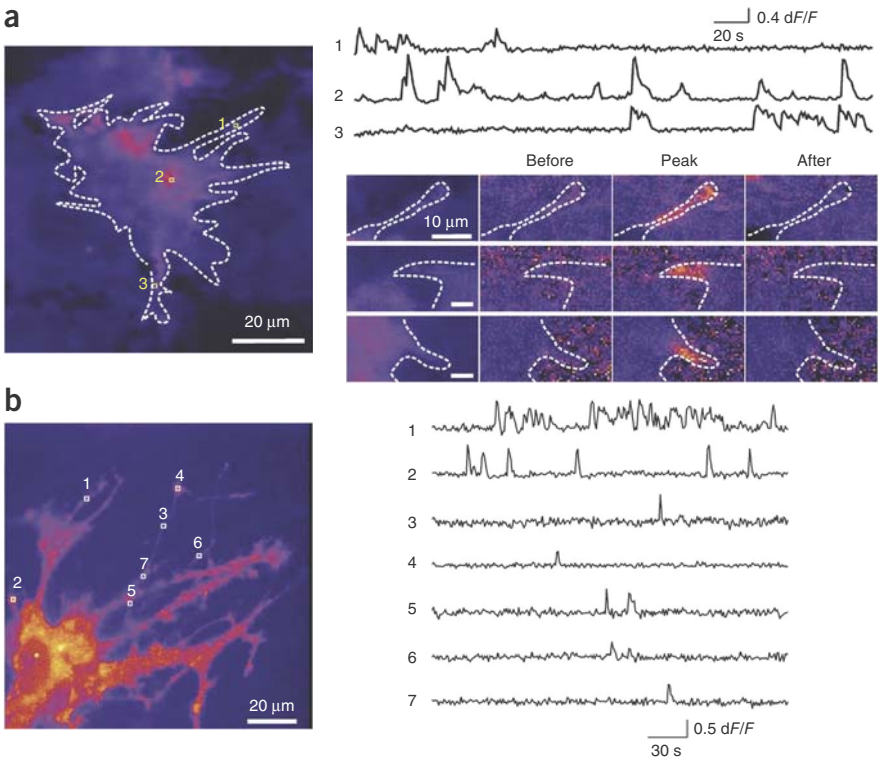

Figure 7 Spotty calcium signals measured in astrocyte processes. (**a**) Image of an astrocyte with its outline superimposed and three regions of interest indicated as 1–3. Right, the d*F*/*F* of Lck-GCaMP2 fluorescence was plotted over time for 1–3. The lower right images give three further examples of localized calcium signals occurring in processes, independent of those in the cell body; note, processes were readily visible. (**b**) Image of an astrocyte treated with 5 mM db-cAMP for 48 h to extend processes; note the longer processes as compared to the image in **a** (**Supplementary Fig. 2**). Right, d*F*/*F* over time for seven microdomain signals.

microdomains in astrocytes were resistant to TTX (**Fig. 8**). Fourth, Lck-GCaMP2 was equally well expressed in neurons and astrocytes (**Supplementary Table 1**). Overall, our data indicate that microdomain calcium signals recorded in astrocytes with Lck-GCaMP2 are unlike signals measured in neurons.

Given that astrocytes in culture have intracellular vesicles and given that application of Lck-GCaMP2 results in uniform labeling of the plasma membrane (**Supplementary Fig. 1**), we next determined whether movement of fluorescent vesicles into a region of interest (ROI) could account for microdomain calcium signals (**Supplementary Fig. 5**). First, the microdomains were abolished by removing extracellular calcium (**Fig. 8**), which is strong evidence for transmembrane calcium fluxes rather than vesicle movement. Second, using Lck-GFP, the d*F*/*F* values resulting from vesicle movement into an ROI were tenfold smaller than d*F*/*F* values for microdomains measured with Lck-GCaMP2 (**Supplementary Fig. 5** and **Supplementary Video 7**). Third, the FWHM of Lck-GFP–labeled vesicles was at the resolution of our microscope at ~400 nm (**Supplementary Fig. 5**), whereas microdomains displayed FWHM of ~5 µm (**Fig. 6d**). Thus, vesicle movement can not account for the microdomain calcium signals measured with Lck-GCaMP2.

We also considered the possibility that the astrocyte membrane may be tortuous, leading to more Lck-GCaMP2 in spots, which may, in turn, lead to more robust calcium signals in these areas. We measured the fluorescence intensity of ROIs encompassing microdomains before they occurred and compared these values with those of the two nearest ROIs (2 and 5 µm away; **Supplementary Fig. 6**). We found that the basal fluorescence intensity of Lck-GCaMP2 was not different from that of the nearest ROIs that did not display microdomains. Within the limits of resolution, these data suggest that microdomain calcium signals are not a result of local accumulation of Lck-GCaMP2 (**Supplementary Fig. 6**).

We further characterized Lck-GCaMP2 expression in astrocytes (**Supplementary Fig. 7**). First, we found that Lck-GCaMP2 was mainly expressed in the plasma membrane (**Supplementary Fig. 7**), where it was ~14-fold more abundant than GCaMP2 (**Supplementary Fig. 7**). Second, the mobility of Lck-GCaMP2 was substantially lower than that of cytosolic GCaMP2 (**Supplementary Fig. 7**). Thus, our results suggest that high plasma membrane expression of a slowly diffusible indicator renders Lck-GCaMP2 well suited to measure localized spontaneous microdomain calcium signals near the membrane and in restricted volumes of astrocyte processes on a timescale of seconds (**Figs. 6**–**8**).

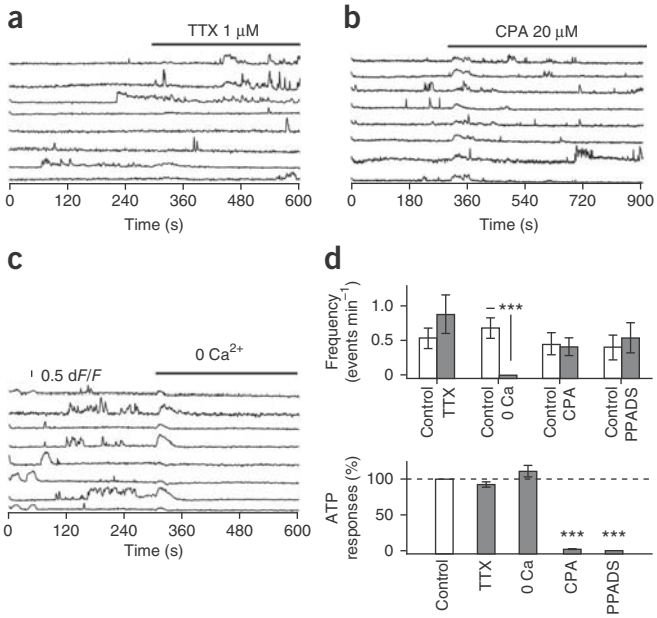

Figure 8 Microdomain signals are a result of transmembrane calcium flux. (**a**) Representative d*F*/*F* traces of microdomains measured with Lck-GCaMP2. TTX (1 µM) was applied at the bar for 5 min. (**b**,**c**) Data are presented as in **a** for CPA (20 µM, **b**) or calcium-free buffer (**c**). (**d**) Top, summary data for microdomain frequency in cells treated with the indicated drugs. Bottom, peak ATP responses relative to control for the same drugs. Error bars represent s.e.m. ***$P < 0.001$.

© 2010 Nature America, Inc. All rights reserved.

DISCUSSION

We developed Lck-GCaMP2, a genetically targeted calcium sensor that is tethered to the plasma membrane, and used it to monitor distinct and previously unknown types of calcium signals in astrocytes, including signals localized in fine processes. In hippocampal astrocyte-neuron cocultures, Lck-GCaMP2 detected near membrane calcium signals evoked pharmacologically or by single action potential–mediated neurotransmitter release. Lck-GCaMP2 also revealed highly localized, frequent spontaneous calcium signals in astrocyte somata and processes that conventional GCaMP2 failed to detect. We used TIRF microscopy in our characterization experiments because it offers excellent axial resolution for studying signaling near the plasma membrane[36]. By necessity, we used cultured astrocytes, as TIRF can only be performed on cells that are attached to glass coverslips[36]. Although astrocytes in culture differ from those *in vivo*[48], we believe that this does not detract from our finding that Lck-GCaMP2 is able to monitor calcium signaling near the plasma membrane and in fine processes of astrocytes.

The potential role of calcium signaling in distal astrocyte processes is important and understudied. Each hippocampal astrocyte may contact up to 100,000 synapses via its fine processes[16]. Calcium transients have mostly been measured from somatic regions of astrocytes. It remains unclear whether distal astrocyte processes have similar transients, whether calcium transients are compartmentalized or whether they are synchronous with the somatic regions. We attempted to measure differences between the soma and processes of astrocytes conventionally with Fluo-4 in acute hippocampal slices and found that calcium transients appeared to be compartmentalized in astrocyte branches (**Supplementary Fig. 8**). These observations are consistent with previously published work[32,33] and support the hypothesis that local compartmentalized calcium transients exist in astrocyte branches. However, these and other data are limited because the volume of the astrocyte processes is too meager to adequately load with calcium indicator dyes, highlighting the need for alternative approaches, such as Lck-GCaMP2. It is noteworthy that the microdomain calcium signals that we found in astrocyte processes using Lck-GCaMP2 are distinct from previous studies in Bergmann glia, which had microdomain-like signals as a result of calcium release from intracellular stores[33]. Thus, our finding of a membrane calcium flux pathway detected by Lck-GCaMP2 (**Figs. 7** and **8**) supports the emerging view that astroglia signal locally via their processes[18].

Using cytosolic GCaMP2, we failed to detect spontaneous, presumably physiological, astrocyte calcium transients[32]. Although cytosolic GCaMP2 can detect pharmacologically evoked calcium signals, we believe such pharmacological GPCR-mediated signals are less interesting and probably represent nonphysiological activation of astrocytes. Using nearly simultaneous EPI and TIRF microscopy, we found that pharmacologically evoked signals were fundamentally different in terms of amplitude and spatial spread in relation to spontaneous calcium signals, which were smaller and more restricted. The possibility that pharmacologically evoked calcium signals may be nonphysiological has previously been raised[15,29].

Our characterization and proof-of-principle experiments indicate that Lck-GCaMP2 is a substantial improvement over cytosolic GCaMP2 for detecting microdomain calcium signals in astrocytes. This approach can now be used to understand the settings in which calcium signals occur in individual astrocytes, which astrocytes display calcium signals in intact networks, and whether astrocyte processes generate calcium signals at their contact points with synapses and blood vessels. Our findings with membrane-targeted Lck-GCaMP2 do not detract from recent work using expression of the cytosolic FRET-based calcium sensor yellow cameleon 3.6 (YC3.6) in astrocytes[49]. However, cytosolic YC3.6 expression may be best suited to study astrocyte cell bodies, as astrocyte processes were revealed as a "hazy cloud." Moreover, we believe our approach is simpler to implement, as Lck-GCaMP2 relies on a single wavelength for excitation (488 nm) and has a single emission peak (508 nm), making it ideal for standard single and multiphoton microscopes. Our data also suggest that, by virtue of the membrane tether, Lck-GCaMP2 is better suited to image calcium in fine processes. TIRF microscopy indicated that Lck-GCaMP2 was uniformly and predominantly expressed in the plasma membrane and was present at high levels in astrocyte processes that have a high plasma membrane–to-volume ratio. Finally, the restricted mobility of Lck-GCaMP2 renders it better suited to detecting local point source–like calcium signals that arise as a result of calcium entry across the plasma membrane[50].

We found that Lck-GCaMP2 was efficiently targeted to the plasma membrane and functioned similar to native GCaMP2 in terms of calcium affinity and sensitivity[39]. To the best of our knowledge, the Lck domain has not previously been used to target a calcium sensor to the plasma membrane, although its membrane targeting ability has been reported[41,42]. Our data indicate that Lck efficiently recruited GCaMP2 to the plasma membrane, probably because it contains tandem palmitoylation and myristoylation domains. Fluorescent proteins are continually being improved by redesign and mutagenesis. Recent modification of GCaMP2 to GCaMP3 led to a threefold improved expression and signal-to-noise ratio that enabled tracking of spontaneous action potentials missed with GCaMP2 (ref. 43). In comparison, Lck-GCaMP2 improves near-surface expression in astrocytes by ~14-fold and improved the signal-to-noise ratio, resulting in the detection of spontaneous calcium signals not detected by cytosolic GCaMP2. In future studies, this Lck based strategy may be useful for determining the utility of new generations of genetically encoded calcium indicators.

The study of astrocyte calcium signaling and its potential effect on neuronal function is growing rapidly, but there are important unresolved issues. First, it is necessary to monitor astrocyte calcium signals in distal processes that contact synapses to test hypotheses on the role of astrocytes during synaptic transmission and plasticity[15,27,29]. Second, it is necessary to monitor calcium signaling in astrocyte endfeet near blood vessels and relate these to vessel constriction and/or dilation[5,6]. It will be important to extend our approach further by generating transgenic mice that express Lck-GCaMP2 selectively in astrocytes. Third, Lck-GCaMP2 will be useful to identify the molecular basis of calcium signals in astrocytes using genome wide or targeted siRNA libraries. Technical advances often lead to breakthroughs in understanding complex problems; we believe that use of Lck-GCaMP2 *in vitro* and *in vivo* will reveal precisely how, when and where local calcium signaling occurs in astrocyte processes with relevance for astrocyte function, not only in healthy circuits, but also during reactive astrogliosis in specific injury and disease contexts[3]. Finally, Lck-GCaMP2 is likely to be useful for monitoring calcium signaling in other glial cells[28] (oligodendrocytes, NG2 cells, Schwann cells, microglia), and thus add to the repertoire of available methods for exploring their roles in brain.

METHODS

Methods and any associated references are available in the online version of the paper at http://www.nature.com/natureneuroscience/.

Note: Supplementary information is available on the Nature Neuroscience website.

© 2010 Nature America, Inc. All rights reserved.

ACKNOWLEDGMENTS

We thank L. Looger for a preprint of a manuscript on GCaMP3, A. Sagasti for the GCaMP2 plasmid, D.E. Bergles for insightful discussions and for the Lck domain plasmid, and M. Simon for MrgA1-EGFP. Our work was supported by the National Institutes of Health (NS060677 and NS057624), the Whitehall Foundation, a S&R Foundation Ryuji Ueno Award for Ion Channels or Barrier Function Research and a Stein-Oppenheimer Foundation Endowment Award (B.S.K.). E.S. was partly supported by the Uehara Memorial Foundation Fellowship of Japan.

AUTHOR CONTRIBUTIONS

E.S. carried out all of the imaging experiments. S.K. carried out all of the cloning experiments. All of the authors contributed to the writing of the manuscript. E.S. and B.S.K. constructed the figures. B.S.K. directed the research with feedback from M.V.S.

COMPETING FINANCIAL INTERESTS

The authors declare no competing financial interests.

Published online at http://www.nature.com/natureneuroscience/.
Reprints and permissions information is available online at http://www.nature.com/reprintsandpermissions/.

1. Kofuji, P. & Newman, E.A. Potassium buffering in the central nervous system. *Neuroscience* **129**, 1045–1056 (2004).
2. Magistretti, P.J. Neuron-glia metabolic coupling and plasticity. *J. Exp. Biol.* **209**, 2304–2311 (2006).
3. Sofroniew, M.V. Molecular dissection of reactive astrogliosis and glial scar formation. *Trends Neurosci.* **32**, 638–647 (2009).
4. Araque, A., Parpura, V., Sanzgiri, R.P. & Haydon, P.G. Tripartite synapses: glia, the unacknowledged partner. *Trends Neurosci.* **22**, 208–215 (1999).
5. Iadecola, C. & Nedergaard, M. Glial regulation of the cerebral microvasculature. *Nat. Neurosci.* **10**, 1369–1376 (2007).
6. Gordon, G.R., Mulligan, S.J. & MacVicar, B.A. Astrocyte control of the cerebrovasculature. *Glia* **55**, 1214–1221 (2007).
7. Cornell-Bell, A.H., Finkbeiner, S.M., Cooper, M.S. & Smith, S.J. Glutamate induces calcium waves in cultured astrocytes: long-range glial signaling. *Science* **247**, 470–473 (1990).
8. Hirase, H., Qian, L., Bartho, P. & Buzsaki, G. Calcium dynamics of cortical astrocytic networks *in vivo*. *PLoS Biol.* **2**, e96 (2004).
9. Wang, X. *et al.* Astrocytic Ca(2+) signaling evoked by sensory stimulation *in vivo*. *Nat. Neurosci.* **9**, 816–823 (2006).
10. Bekar, L.K., He, W. & Nedergaard, M. Locus coeruleus alpha-adrenergic–mediated activation of cortical astrocytes *in vivo*. *Cereb. Cortex* **18**, 2789–2795 (2008).
11. Dombeck, D.A., Khabbaz, A.N., Collman, F., Adelman, T.L. & Tank, D.W. Imaging large-scale neural activity with cellular resolution in awake, mobile mice. *Neuron* **56**, 43–57 (2007).
12. Göbel, W., Kampa, B.M. & Helmchen, F. Imaging cellular network dynamics in three dimensions using fast 3D laser scanning. *Nat. Methods* **4**, 73–79 (2007).
13. Schummers, J., Yu, H. & Sur, M. Tuned responses of astrocytes and their influence on hemodynamic signals in the visual cortex. *Science* **320**, 1638–1643 (2008).
14. Oberheim, N.A. *et al.* Uniquely hominid features of adult human astrocytes. *J. Neurosci.* **29**, 3276–3287 (2009).
15. Fiacco, T.A., Agulhon, C. & McCarthy, K.D. Sorting out astrocyte physiology from pharmacology. *Annu. Rev. Pharmacol. Toxicol.* **49**, 151–174 (2009).
16. Bushong, E.A., Martone, M.E., Jones, Y.Z. & Ellisman, M.H. Protoplasmic astrocytes in CA1 stratum radiatum occupy separate anatomical domains. *J. Neurosci.* **22**, 183–192 (2002).
17. Halassa, M.M., Fellin, T., Takano, H., Dong, J.H. & Haydon, P.G. Synaptic islands defined by the territory of a single astrocyte. *J. Neurosci.* **27**, 6473–6477 (2007).
18. Gordon, G.R. *et al.* Astrocyte-mediated distributed plasticity at hypothalamic glutamate synapses. *Neuron* **64**, 391–403 (2009).
19. Porter, J.T. & McCarthy, K.D. Hippocampal astrocytes *in situ* respond to glutamate released from synaptic terminals. *J. Neurosci.* **16**, 5073–5081 (1996).
20. Parpura, V. *et al.* Glutamate-mediated astrocyte-neuron signaling. *Nature* **369**, 744–747 (1994).
21. Pasti, L., Volterra, A., Pozzan, T. & Carmignoto, G. Intracellular calcium oscillations in astrocytes: a highly plastic, bidirectional form of communication between neurons and astrocytes *in situ*. *J. Neurosci.* **17**, 7817–7830 (1997).
22. Perea, G., Navarrete, M. & Araque, A. Tripartite synapses: astrocytes process and control synaptic information. *Trends Neurosci.* **32**, 421–431 (2009).
23. Lee, C.J. *et al.* Astrocytic control of synaptic NMDA receptors. *J. Physiol. (Lond.)* **581**, 1057–1081 (2007).
24. Fellin, T. *et al.* Neuronal synchrony mediated by astrocytic glutamate through activation of extrasynaptic NMDA receptors. *Neuron* **43**, 729–743 (2004).
25. Fiacco, T.A. *et al.* Selective stimulation of astrocyte calcium *in situ* does not affect neuronal excitatory synaptic activity. *Neuron* **54**, 611–626 (2007).
26. Petravicz, J., Fiacco, T.A. & McCarthy, K.D. Loss of IP3 receptor–dependent Ca^{2+} increases in hippocampal astrocytes does not affect baseline CA1 pyramidal neuron synaptic activity. *J. Neurosci.* **28**, 4967–4973 (2008).
27. Tritsch, N.X. & Bergles, D.E. Defining the role of astrocytes in neuromodulation. *Neuron* **54**, 497–500 (2007).
28. Barres, B.A. The mystery and magic of glia: a perspective on their roles in health and disease. *Neuron* **60**, 430–440 (2008).
29. Agulhon, C. *et al.* What is the role of astrocyte calcium in neurophysiology? *Neuron* **59**, 932–946 (2008).
30. Lee, S.Y. & Haydon, P.G. Astrocytic glutamate targets NMDA receptors. *J. Physiol. (Lond.)* **581**, 887–888 (2007).
31. Shigetomi, E., Bowser, D.N., Sofroniew, M.V. & Khakh, B.S. Two forms of astrocyte calcium excitability have distinct effects on NMDA receptor-mediated slow inward currents in pyramidal neurons. *J. Neurosci.* **28**, 6659–6663 (2008).
32. Nett, W.J., Oloff, S.H. & McCarthy, K.D. Hippocampal astrocytes in situ exhibit calcium oscillations that occur independent of neuronal activity. *J. Neurophysiol.* **87**, 528–537 (2002).
33. Grosche, J. *et al.* Microdomains for neuron-glia interaction: parallel fiber signaling to Bergmann glial cells. *Nat. Neurosci.* **2**, 139–143 (1999).
34. Bush, T.G. *et al.* Fulminant jejuno-ileitis following ablation of enteric glia in adult transgenic mice. *Cell* **93**, 189–201 (1998).
35. Pascual, O. *et al.* Astrocytic purinergic signaling coordinates synaptic networks. *Science* **310**, 113–116 (2005).
36. Jaiswal, J.K. & Simon, S.M. Imaging single events at the cell membrane. *Nat. Chem. Biol.* **3**, 92–98 (2007).
37. Parpura, V. & Haydon, P.G. Physiological astrocytic calcium levels stimulate glutamate release to modulate adjacent neurons. *Proc. Natl. Acad. Sci. USA* **97**, 8629–8634 (2000).
38. Nakai, J., Ohkura, M. & Imoto, K. A high signal-to-noise Ca^{2+} probe composed of a single green fluorescent protein. *Nat. Biotechnol.* **19**, 137–141 (2001).
39. Tallini, Y.N. *et al.* Imaging cellular signals in the heart *in vivo*: Cardiac expression of the high-signal Ca^{2+} indicator GCaMP2. *Proc. Natl. Acad. Sci. USA* **103**, 4753–4758 (2006).
40. Mao, T., O' Connor, D.H., Scheuss, V., Nakai, J. & Svoboda, K. Characterization and subcellular targeting of GCaMP-type genetically encoded calcium indicators. *PLoS One* **3**, e1796 (2008).
41. Zlatkine, P., Mehul, B. & Magee, A.I. Retargeting of cytosolic proteins to the plasma membrane by the Lck protein tyrosine kinase dual acylation motif. *J. Cell Sci.* **110**, 673–679 (1997).
42. Benediktsson, A.M., Schachtele, S.J., Green, S.H. & Dailey, M.E. Ballistic labeling and dynamic imaging of astrocytes in organotypic hippocampal slice cultures. *J. Neurosci. Methods* **141**, 41–53 (2005).
43. Tian, L. *et al.* Imaging neural activity in worms, flies and mice with improved GCaMP calcium indicators. *Nat. Methods* **6**, 875–881 (2009).
44. Shigetomi, E. & Khakh, B.S. Measuring near plasma membrane and global intracellular calcium dynamics in astrocytes. *J. Vis. Exp.* **26**, 10.3791/1142 (2009).
45. Richler, E., Chaumont, S., Shigetomi, E., Sagasti, A. & Khakh, B.S. An approach to image activation of transmitter-gated P2X receptors *in vitro* and *in vivo*. *Nat. Methods* **5**, 87–93 (2008).
46. Goldman, J.E. & Abramson, B. Cyclic AMP-induced shape changes of astrocytes are accompanied by rapid depolymerization of actin. *Brain Res.* **528**, 189–196 (1990).
47. Oberheim, N.A. *et al.* Loss of astrocytic domain organization in the epileptic brain. *J. Neurosci.* **28**, 3264–3276 (2008).
48. Cahoy, J.D. *et al.* A transcriptome database for astrocytes, neurons, and oligodendrocytes: a new resource for understanding brain development and function. *J. Neurosci.* **28**, 264–278 (2008).
49. Atkin, S.D. *et al.* Transgenic mice expressing a cameleon fluorescent Ca^{2+} indicator in astrocytes and Schwann cells allow study of glial cell Ca^{2+} signals *in situ* and *in vivo*. *J. Neurosci. Methods* **181**, 212–226 (2009).
50. Reyes, R.C. & Parpura, V. The trinity of Ca^{2+} sources for the exocytotic glutamate release from astrocytes. *Neurochem. Int.* **55**, 2–8 (2009).

© 2010 Nature America, Inc. All rights reserved.

ONLINE METHODS

Molecular biology. The GCaMP2 sequence was removed from the plasmid pN1 GCaMP2 by restriction digest using the 5′ BglII site followed by Klenow treatment (to create a blunt end) and the 3′ NotI site. This fragment was then ligated into a plasmid containing the N-terminal 26 amino acid sequence of Lck (pN1 Lck-EGFP, kind gift from D.E. Bergles, Johns Hopkins University), from which the EGFP coding sequence was removed by restriction digest, using AgeI (5′) followed by Klenow treatment and NotI (3′). This created Lck-GCaMP2; all constructs were verified by DNA sequencing.

HEK-293 cell culture. HEK-293 cells (obtained from ATCC) were maintained in 75-cm^2 cell culture flasks in DMEM/F12 media with Glutamax (Invitrogen) supplemented with 10% fetal bovine serum (vol/vol) and penicillin/streptomycin. Cells were grown in a humidified atmosphere of 95% air/5% CO_2 at 37 °C in a cell culture incubator. The cells were split 1 in 10 when confluence reached 60–90%, which was generally every 3 to 4 d. Cells were prepared for transfection by plating onto six-well plates at the time of splitting 3–4 d before transfection. They were transfected at 60–90% confluence. For transient expression in HEK-293, we used 0.5–1 μg plasmid cDNA and the Effectene transfection reagent (Qiagen) for each well of a six-well plate. The manufacturer's instructions were followed with 4 μl of enhancer and 10 μl of Effectene used for each transfection. Buffered calcium solutions used for determining the calcium K_d of Lck-GCaMP2 were made in HEK cell buffer (150 mM NaCl, 1 mM $MgCl_2$, 10 mM D-glucose, 10 mM HEPES and 1 mM EGTA at pH 7.5, adjusted with NaOH) with the aid of the MaxChelator program (http://www.stanford.edu/~cpatton/maxc.html) to calculate the amount of $CaCl_2$ added to achieve a particular final concentration. To achieve permeablization, we treated cells with 0.1% Triton X-100 (vol/vol, without calcium) for 15–30 s. The cells were then washed three times with zero calcium buffer and imaged.

EPI and TIRF microscopy. Briefly, we used an Olympus IX71 microscope equipped with an IXON DV887DCS EMCCD camera (Andor) or a RETIGA 2000DC camera (QImaging), EPI condenser, control unit and Polychrome V monochromator (TILL Photonics). The control of excitation and image acquisition was achieved using TILLVision software (TILL Photonics). The beams of 454-, 488- and 515-nm argon (100 mW) and 442-nm solid state (45 mW) lasers was combined and controlled with a TILL Polyline laser combiner, TIRF dual port condenser and acoustoptical tuneable filter and controller (TILL Photonics) and fed into a Kineflex broadband fiber for entry into the TIRF condenser. We used an Olympus 60× 1.45 NA lens to achieve TIRF. Some experiments were carried with a similar setup using a Peltier cooled (−15 °C) Imago CCD camera (reduced to 640 × 480 pixels, each pixel 9.9 × 9.9 μm), EPI condenser, control unit (containing ISC and PDC boards) and the Polychrome IV monochromator (TILL Photonics), and the cells were viewed a 40× water-immersion objective lens with a numerical aperture of 0.8 (Olympus).

Calcium imaging. For calcium imaging with organic calcium indicator dyes, astrocytes were loaded with Fluo-4/AM (2.5 μM, Invitrogen) or Fura-2/AM (10 μM, Invitrogen) for 10–30 min. We used 0.05% Pluronic F-127 20% solution (vol/vol) in DMSO (Invitrogen) to facilitate loading organic calcium indicators. Images were typically taken every 1 s. Exposure time and pixel binning were optimized to visualize fluorescence signals for each experiment (maximum binning was 4 × 4). Cultures were perfused with recording buffer (110 mM NaCl, 5.4 mM KCl, 1.8 mM $CaCl_2$, 0.8 mM $MgCl_2$, 10 mM D-glucose and 10 mM HEPES at pH 7.4, adjusted with NaOH).

Hippocampal astrocyte-neuron cultures. Hippocampal cultures were prepared as described previously[44]. Briefly, two rat pups at P1 or P2 (Charles River) were used for hippocampal cultures. Hippocampi were dissected in Petri dishes filled with ice-cold medium. The dissected hippocampi (in medium, on ice) were cut and then digested with 20 U ml^{-1} papain for 11–13 min at 37 °C (papain-022, Worthington). After the incubation, the pieces were washed with pre-warmed media and triturated with flame-polished pipettes of progressively smaller bores; 120,000 (for 22 mm coverslips, VWR) or 20,000 cells (for 12 mm coverslips, VWR) were used for plating onto each coverslip. The coverslips were previously coated with poly-D-lysine (50 μg ml^{-1}, Sigma) and then overnight with 400 (for 22-mm coverslips) or 100 μl (for 12-mm coverslips) of 20 μg ml^{-1} laminin (Sigma) in sterile dissection medium. The cells were fed with 2 ml of pre-warmed culture medium 1 h after plating.

Astrocyte and neuron transfection. Before transfection, half of the media was removed and the astrocytes were fed with fresh media that had been pre-warmed to 37 °C for more than 30 min. The removed media was supplemented with an equal volume of new media and stored in the cell culture incubator (this is the fed and conditioned medium). For EFS experiments, we used Neurobasal-based media to keep neurons healthy. We transfected astrocytes at 4–6 d in culture with the Effectene transfection reagent (Qiagen). We typically used 0.6–1 μg of DNA, 3.2 μl enhancer and 10 μl Effectene for each well of a six-well plate. After 12–24 h, the medium was removed from each well and replaced with 2 ml of the fed and conditioned medium. Experiments were carried out within 3 d of transfection.

Agonist applications and electrical field stimulation. Drugs were applied to single cells using a Warner Instrument VC-8 valve controller or to all cells on the glass coverslip in the bathing medium (at 2–3 ml min^{-1}). We used a microscope stage–mounted glass bottom chamber with built in platinum electrodes (Warner Instruments) connected to a Grass S88 stimulator for field stimulation as previously described[45]. We used a pulse width of 100 μs and stimulation frequency of 30 Hz (stimulus intensity was 85–90 V). For EFS experiments, we used a static bath.

FM1-43 staining. The plasma membranes of astrocytes were stained with FM1-43 (5 μg ml^{-1}, Invitrogen) according to manufacturer's protocol. Briefly, coverslips were mounted on the TIRF microscope and then incubated with ice-cold FM1-43 staining solution for 1 min. Images were taken immediately after staining within 15 min.

Calcium imaging in brain slices. Coronal slices of the hippocampus from young rats (P10–20) were cut and incubated at 20–25 °C in artificial cerebrospinal fluid (aCSF: 126 mM NaCl, 2.5 mM KCl, 1.3 mM $MgCl_2$, 10 mM D-glucose, 2.4 mM $CaCl_2$, 1.24 mM NaH_2PO_4 and 26 mM $NaHCO_3$, saturated with 95% O_2 and 5% CO_2). Brain slices were loaded at 20–25 °C in the dark with 5 μM Fluo-4/AM in aCSF for 60 min, then transferred to dye-free aCSF for at least 30 min before experimentation to allow for cleavage of the AM ester group. Live astrocytes were predominantly loaded with the fluorescent dye with these conditions. This was confirmed by infrared differential-interference contrast images of astrocytes in the same area. Images of cells were acquired using an Olympus Fluoview 300 laser-scanning confocal microscope with a 300-mW argon laser, at 2% power every 0.2 s. Emitted green fluorescence was collected through a 510-nm long-pass filter.

Fluorescence recovery after photobleaching. Fluorescence recovery after photobleaching (FRAP) was carried out as described previously[45] using an Olympus BX61WI and FV300 Fluoview confocal laser-scanning microscope. Bleaching was achieved with 100% laser power for ~4 s, followed by examination of recovery every 0.3 s with the laser power at 0.1% of maximum. For these experiments, we used the 488-nm laser line of an argon laser and a 40× objective lens with a numerical aperture of 0.8 (Olympus). Single exponential fits (Origin 8) were used to measure the FRAP time constant (τ), and the apparent diffusion coefficient (D) was estimated using the function $D = \frac{0.224r^2}{t_d}$, where r is the radius of the area that was bleached and t_d is the time taken for FRAP to recover to half of its final value ($t_d = \ln 2\tau$). The average distance (d) traveled in two dimensions in time (t) was estimated as $d = \sqrt{4Dt}$.

Immunofluorescence microscopy. Cultures were fixed with 1:1 solution of freshly prepared acetone and methanol for 5 min and then incubated for 7 min with phosphate-buffered saline (PBS) containing 0.25% Triton X-100. After blocking nonspecific binding sites with 10% normal goat serum (vol/vol) for 30 min, cultures were incubated with rabbit polyclonal antibody to GFAP (1:10,000, DAKO) in 2% normal goat serum overnight at 4 °C. After washing unbound antibody with PBS three times, cultures were incubated with Alexa 488–conjugated goat antibody to rabbit IgG (1:500, Invitrogen). Cultures were washed with PBS three times and then fluorescence images were taken using Olympus BX61WI microscope and FV300 Fluoview confocal laser-scanning head.

Data analysis. Image analysis was performed with ImageJ (US National Institutes of Health). All statistical tests were run in Origin 8 (OriginLab), which was also used for creating graphs. The figures were assembled in CorelDraw 12. Data are presented as mean ± s.e.m.

© 2010 Nature America, Inc. All rights reserved.